The 19th Cambridge Workshop on Cool Stars, Stellar Systems, and the Sun
Edited by G. A. Feiden

Swift observations of CC Eri: X-ray superflare

Subhajeet Karmakar & Jeewan C. Pandey

Aryabhatta Research Institute of observational sciencES (ARIES), Nainital-263002, India

Abstract

We present analysis of a superflare detected on an active binary system CC Eridani by *Swift* observatory. The flare (F1) triggered the Burst Alert Telescope (BAT) in the hard X-ray band on 2008 October 16. The rise-phase was observed only with BAT, whereas the decay phase was observed simultaneously with X-Ray Telescope (XRT). The e-folding decay time indicates a faster decay in the hard X-ray band than in the soft X-ray band. Spectral analysis indicates a presence of three temperature corona with first two plasma temperatures remain constant during the flare at $\sim$3 and $\sim$10 MK. The flare-temperature peaked at 342 MK which is $\sim$4 times more than the minimum value observed at post-flaring (PF) phase. The abundances peaked at 2 times the solar abundances, which is also $\sim$11 times larger than the quiescent-state value. Using hydrodynamic loop modeling we derive a loop-length of $1.25\pm0.13\times10^{10}$ cm. The peak X-ray luminosity for flares F1 in the 0.3–50 keV energy band (excluding 10–14 keV band) reached up to $\sim4\times10^{32}$ erg s^{-1}, which is $\sim$3500 times more than the quiescent value and larger than any other flares previously observed on CC Eri.

1 Introduction

Solar and stellar flares are generally interpreted as a rapid and transient release of magnetic energy in corona by reconnection process, associated with electromagnetic radiation from radio waves to γ-rays. The typical total energy of a normal solar flare ranges from 10^{29-32} erg (e.g., Shibata & Yokoyama, 2002; Emslie *et al.*, 2004), whereas the "superflares" on late-type stars generally have a total energy range of 10^{33-38} erg (Schaefer *et al.*, 2000; Shibayama *et al.*, 2013). Few X-ray superflares have been observed in late-type stars such as Algol (Favata & Schmitt, 1999), AB Dor (Maggio *et al.*, 2000), EV Lac (Favata *et al.*, 2000; Osten *et al.*, 2010), UX Ari (Franciosini *et al.*, 2001), II Peg (Osten *et al.*, 2007), and DG CVn (Fender *et al.*, 2015). These extreme flare events are very useful to understand the extent to which the dynamic behavior can vary within the stellar environments. The time-resolved spectral analysis reveals the changes in the characteristics of the flaring plasma, such as the hydrodynamic decay timescales in sustained heating framework, spatial scales, and provide evidence for temporary enrichment of coronal abundances with plasma from the lower layers of the atmosphere. The flaring plasma of superflare was found to consists of high-pressure and high-density coronal loops having a large scale organized magnetic field structure (Favata *et al.*, 2000).

In this paper, we describe a superflare serendipitously observed by *Swift* observatory on an active spectroscopic binary star CC Eri, consists of a K7.5Ve primary and M3.5Ve secondary (Amado *et al.*, 2000), and located at a distance of $\sim$11.5 pc. With a mass ratio $\approx$2 (Evans, 1959), the system is tidally locked and the primary being one of the fastest rotating K dwarfs in the solar vicinity with a rotation period of 1.56 d. Demircan *et al.* (2006) estimated the age of the CC Eri system to be 9.16 Gyr. The chromospheric emission was found to vary in antiphase with its optical continuum, suggesting the presence of active emission regions associated with starspots (Busko *et al.*, 1977; Amado *et al.*, 2000). The first X-ray detection was done with *HEAO1* showing X-ray luminosity (L_X) of $10^{29.6}$ erg s^{-1} in the 2–20 keV energy band (Tsikoudi, 1982). Later several X-ray observations were made with other satellites such as *Einstein* IPC (Caillault *et al.*, 1988), *EXOSAT* (Pallavicini *et al.*, 1988). First ever X-ray flare on CC Eri was detected with *ROSAT* satellite (Pan & Jordan, 1995). Later X-ray flares were detected with *XMM-Newton* (Pandey & Singh, 2008; Crespo-Chacón *et al.*, 2007), *Chandra* (Nordon & Behar, 2007), *Swift* (Evans *et al.*, 2008; Barthelmy *et al.*, 2012), and *MAXI* GCS (Suwa *et al.*, 2011). The time-resolved analysis of CC Eri using *XMM-Newton* data (Pandey & Singh, 2008) indicates that the quiescent corona of CC Eri is well described by two-temperature plasma ($\sim$3 and $\sim$10 MK), with a quiescent state luminosity of $\sim10^{29}$ erg s^{-1} in 0.3–10 keV energy band. Among the previously observed flares, the largest one was observed with *Chandra*, having a peak flux $\sim$11 times larger than the quiescent value. Large-scale surface magnetic fields was estimated by Bopp & Evans (1973) suggesting an existence of large scale organized magnetic field, which can store a large amount of magnetic energy, that can be released in the form of a superflare.

The paper is structured as follows: Observations and the data reduction procedure are discussed in § 2. Analysis and results from X-ray timing and spectral analysis along with the time-resolved spectroscopy, and loop modeling are discussed in § 3. Finally, in § 4 we discuss our results and present conclusions.

2 Observations and data reduction

2.1 BAT Data

The flare F1 triggered *Swift*'s Burst Alert Telescope (BAT; Barthelmy *et al.*, 2005) on 2008 October 16 UT 11:22:52 (=$T0_1$) during a preplanned spacecraft slew. We used BAT pipeline

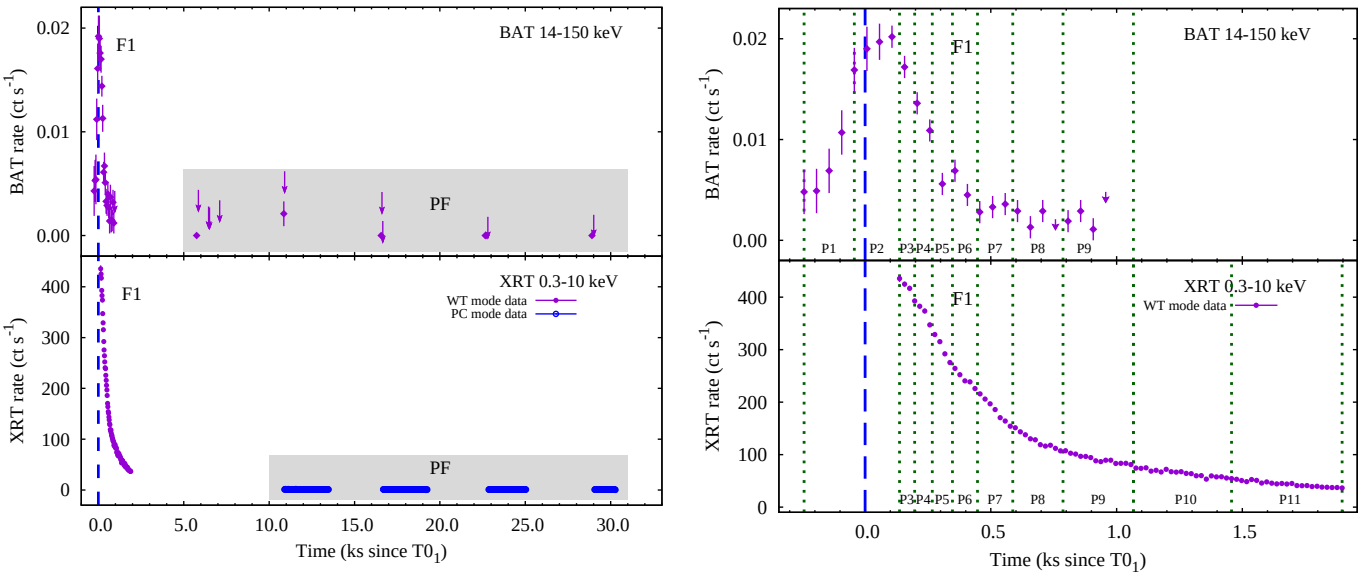

(a) Flare F1 followed by a post flare PF region

(b) Close-up view of flare F1

Figure 1: Flare F1 observed with *Swift* BAT (top) and XRT (bottom). Temporal binning for BAT and XRT light curves were 50 s and 10 s, respectively. Dashed vertical lines indicate the trigger time, whereas dotted vertical lines show the time intervals for time resolved spectroscopy.

software within FTOOLS[1] version 6.18 with latest CALDB version 'BAT (20090130)' to correct the energy from the efficient but slightly non-linear on board energy assignment. BAT light curves were extracted using the task BATBINEVT. For the spectral data reported here, the mask-weighted spectra in 14–50 keV band were produced using BATMASKWTEVT and BATBINEVT task with energy bin of 80 channels. The BAT ray tracing columns in spectral files were updated using BATUPDATEPHAKW task, whereas the systematic error vector was applied to the spectra from the calibration database using BATPHASYSERR task. The BAT detector response matrix was computed using BATDRMGEN task. The sky images in two broad energy bins were created using BATBINEVT and BATFFTIMAGE, and flux at the source position was found using BATCELLDETECT, after removing a fit to the diffuse background and the contribution of bright sources in the field of view. Spectral analysis of all the BAT spectra was done using X-ray spectral fitting package (XSPEC; version 12.9.0; Arnaud, 1996). All the errors associated with the fitting of the BAT spectra were calculated for a confidence interval of 68% ($\Delta\chi^2$= 1).

2.2 XRT Data

The X-Ray Telescope (XRT; Burrows *et al.*, 2005) started to observe flare F1 from 147.2 s after $T0_1$. The XRT observes in the energy range of 0.3–10 keV using CCD detectors, with the energy resolution of ≈ 140 eV at Fe K (6 keV) region as measured at launch time. In order to produce the cleaned and calibrated event files, all the data were reduced using the *Swift* XRTPIPELINE task (version 0.13.2) and calibration files from the latest CALDB version 'XRT (20150721)' release [2]. The cleaned event lists generated with this pipeline are free from the effects of hot pixels and the bright Earth. Due to the large XRT count rate of flare F1, the initial data recording was in Windowed Timing (WT) mode; ∼11.7 ks after $T0_1$ to the end of the observation (∼31.1 ks after $T0_1$) data were taken in Photon Counting (PC) mode, spread across four snapshots. From the cleaned event list, images, light curves, and spectra for each observation were obtained with XSELECT (version 2.4c) package. We only use grade 0-2 events in WT mode and grade 0-12 events in PC mode to optimize the effective area and hence the number of collected counts.

In order to correct for the pile-up effect, the source region of WT data were extracted in a rectangular 40×20-pixel region (40 pixels long along the image strip and 20 pixels wide; 1 pixel = 2.36″) with a region of increasing size (0×20–20×20 pixels) excluded from its center, whereas background region was extracted as 40×20-pixel region in the fainter end of image strip. We produced a sample of grade ratio distribution using background-subtracted source event lists created in each region. The grade ratio distribution for grade 0 event is defined as the ratio of grade 0 event over the sum of grade 0–2 events per energy bin in the 0.3–10 keV energy range. Comparing the grade ratio distribution with that obtained using non-piled-up WT data we find that an exclusion of the innermost 5 pixels was necessary for the WT mode data. In PC mode, we fit the wings of the source radial PSF profile with the XRT PSF model (a King function; see Moretti *et al.*, 2005) excluding 15 pixels from the center and then extrapolated to the inner region. The PSF profile of innermost 4 pixels was found to deviate from the King function, exclusion of

[1]The mission-specific data analysis procedures are provided in FTOOLS software package; a full description of the procedures mentioned here can be found at https://heasarc.gsfc.nasa.gov/docs/software/ftools/ftools_menu.html

[2]See http://heasarc.gsfc.nasa.gov/docs/swift/analysis/

which enables us to mitigate the effects of pile-up from PC mode data.

Taking into account the point-spread function correction (PSF; Moretti *et al.*, 2005) as well as the exposure map correction, the *ancillary response files* for the WT and PC modes were produced using the task XRTMKARF. In order to perform the spectral analysis, we used the latest *response matrix files* (Godet *et al.*, 2009) i.e. SWXWT0TO2S6_20010101V015.RMF in WT mode and SWXPC0TO12S6_20010101V014.RMF in PC mode. All XRT spectra were binned to contain more than 20 counts bin^{-1}. The spectral analysis of all the XRT spectra was carried out in an energy range of 0.3 to 10 keV using XSPEC. All the errors of XRT spectral fitting are estimated with 68% confidence interval ($\Delta\chi^2$= 1), equivalent to $\pm1\sigma$. In our analysis the solar photospheric abundances ($Z_\odot$) were adopted from Anders & Grevesse (1989), whereas to model N_H, we used the cross sections obtained by Morrison & McCammon (1983).

3 Results and Analysis

3.1 X-ray light curves

X-ray light curves of CC Eri obtained in 0.3–10 keV and 14–150 keV energy bands are shown in Fig. 1. The BAT observation began at $T0_1$–243 s shows a rise in intensity up to $T0_1$+100 s where it reaches a peak intensity with a count rate of 0.024 $\pm$0.005 counts s^{-1}, which is $\sim$24 times higher than the minimum observed count rate. A sharp decrease in intensity up to nearly $T0_1$+450 s was observed followed by a shallower decay till the end of the BAT observations at $\sim T0_1$+950 s. The XRT count-rate of flare F1 was already declining as it entered the XRT field of view at $T0_1$+142 s. Due to the pile up correction, we lost significant amount of photons, the peak XRT count rate for the pile-up corrected data is found to be 437$\pm$7 counts s^{-1}, which is $\sim$100 counts s^{-1} lower than the previously reported count rate (Evans *et al.*, 2008). Flare F1 was still survived during the $\sim$1.8 ks of WT mode observation, after that, the observation was switched over in PC mode where count rates found to be constant and marked as 'PF' in Fig. 1(a). The XRT count rates at the peak of the flare was found to be 474 times more than those in the post-flare state. The e-folding rise times (τ_r) of the flare F1 derived from BAT data are found to be 150$\pm$12 s; whereas e-folding decay times (τ_d) with BAT and XRT data were found to be 283$\pm$13 and 539$\pm$4 s. This indicates a faster decay in hard X-ray band than in soft X-ray.

3.2 BAT Spectral Analysis

In order to trace the spectral change, we have divided BAT light curve into nine time segments, spectra of each time segments were extracted. The dotted vertical lines in the top panel of Fig. 1(b) indicate the time intervals during which BAT spectra were accumulated. In this section, we analyze only those time segments where only the BAT observations were available, i.e. first two time segments for flare F1 (P1 and P2). The hard X-ray spectra were best-fitted using single temperature Astrophysical Plasma Emission Code (APEC; see Smith *et al.*, 2001) as implemented for collisionally ionized plasma. The addition of another thermal or non-thermal component does not improve the fit-statistics. Since the standard APEC model included in the XSPEC distribution only considers emission up to photon energies of 50 keV; therefore, we restricted our analysis in 14–50 keV energy band. The abundances in this analysis were fixed to the mean abundances derived from XRT spectral fitting (see § 3.3) given in a multiple of the solar values of Anders & Grevesse (1989). The galactic HI Column Density (N_H) in the direction of CC Eri is calculated according to the survey of Dickey & Lockman (1990) and kept fixed at the value of 2.5×10^{20} cm^{-2}. The variation in hard X-ray luminosity ($L_{X,[14-50]}$), plasma temperature (kT), and emission measure (EM), and abundances (Z) derived from the BAT spectra are illustrated in Fig 3. The inferred peak plasma temperatures during the flare was $>$14.4 keV.

3.3 XRT Spectral Analysis

3.3.1 Post-Flare spectra

The coronal parameters of PF phase were derived by fitting single (1T), double (2T), and triple (3T) temperature APEC model. The global abundances (Z) and interstellar HI column density (N_H) were left as free parameters. None of the plasma models (1T, 2T, or 3T) were formally acceptable with a solar photospheric abundances with a large χ^2 value. The 2T and 3T plasma models with sub-solar abundances were found to be significantly better fit, although, the 2T model was not found to be formally acceptable and inspection of residuals showed evidence of line emission near 0.6 keV. Only a 3T plasma model with sub-solar abundances was found to be acceptable with a reduced χ^2 value of 1.14 for 119 degrees of freedom (DOF). The F-test applied to the χ^2 resulting from the fits with APEC 2T and 3T model showed that the 3T model is more significant with a F-statistics of 25.3 and a null hypothesis probability of 6.78×10^{-10}. Addition of one more thermal component did not show any further improvement in the reduced χ^2; therefore, we assume that the post-flare coronae of CC Eri were well represented by three temperatures plasma. The derived value of N_H from the spectral analysis was found to be less than the total galactic HI column density (Dickey & Lockman, 1990) towards the direction of that star. The first two temperatures in 3T model were derived to be $0.25^{+0.02}_{-0.02}$ and $0.94^{+0.03}_{-0.03}$ keV, respectively, which is found to be within 1σ level of the two temperature quiescent corona of CC Eri derived by Crespo-Chacón *et al.* (2007) and Pandey & Singh (2008) using *XMM-Newton* data. This indicates that the post-flaring region has not yet returned to the quiescent level and have a third thermal component of $3.4^{+0.7}_{-0.6}$ keV. With the preliminary analysis of the same data Evans *et al.* (2008) also suspected that the post-flare region is not a quiescent state. Therefore, for further analysis, we considered the first two thermal components as the quiescent components of CC Eri. The corresponding ratio of two quiescent components of emission measure (EM_2/EM_1) was found to be $\sim$1.2. The X-ray luminosity in 0.3–10 keV band during the post-flare region was derived to be $3.81^{+0.03}_{-0.51}\times10^{29}$ erg s^{-1}.

3.3.2 Flare spectra: Time-Resolved Spectroscopy

We performed a detailed time-resolved analysis in order to investigate the evolution of spectral parameters during the soft X-ray flare of the WT mode data. The dotted vertical lines in the bottom panel of Fig. 1(b) show the time intervals for which the X-ray spectra were accumulated. We di-

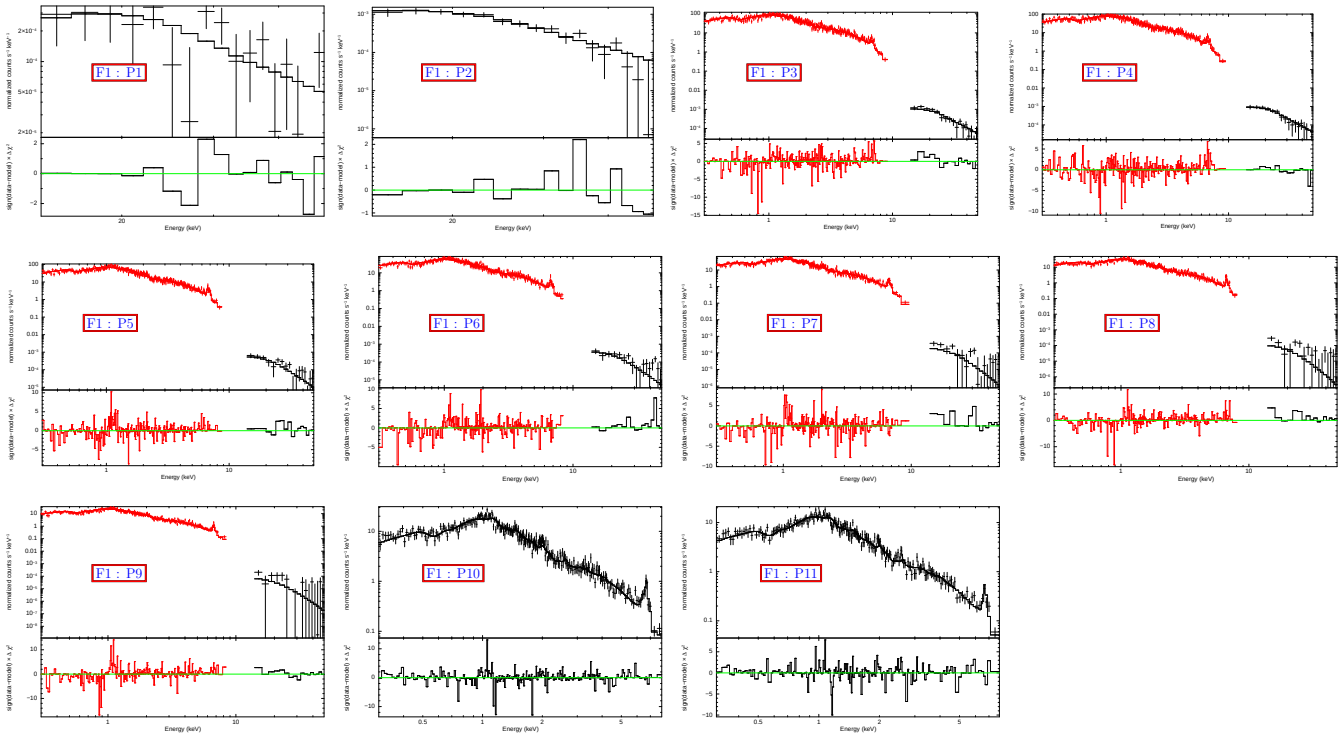

Figure 2: Best-fit APEC model with BAT (P1, P2), XRT+BAT (P3–P9), and XRT (P10, P11) spectra for different time segments mentioned in the top panel of each plot. The bottom panels show the 1σ variation of data from the model.

vided the WT mode data into nine time bins, so that each time bin contains sufficient and similar number of counts after correcting for the pile-up. The length of the time bins is variable, ranging from 60–440 s. The first seven time segments of XRT data were common with BAT data. In order to study the flare emission only, we have performed three temperature spectral fit of the data using the APEC model, with the quiescent emission taken into account by including first two temperatures from PF spectral fitting as a frozen background contribution. This technique allows us to derive one "effective" temperature and one EM of the flaring plasma. Initially, in the spectral fitting N_H was a free parameter and appeared to be constant within a 1σ level to the quiescent state value. Therefore, in next stage of spectral fitting, we fixed N_H to its quiescent state value, along with the two quiescent thermal components. The global abundances, temperature, and corresponding emission measures of the third component were free parameters in spectral fitting. The time evolution of derived spectral parameters of the flare F1 is shown in Fig. 3. The abundance, temperature, and corresponding emission measure were found to vary during the flare. The peak value of abundance was derived to be $2.0^{+0.2}_{-0.3}$ $Z_\odot$, which was $\sim$7 times more than the post-flaring region and $\sim$11 times more than the quiescent value of CC Eri (Pandey & Singh, 2008). The flare temperature peaked at $11.9^{+0.9}_{-0.9}$ keV, which was $\sim$3.5 times more than the third thermal component observed in PF phase. The EM followed the flare light curve and peaked at a value of $12.8^{+0.5}_{-0.5}\times10^{54}$ cm^{-3}, which was respectively $\sim$1424 times more than the minimum value observed at the post-flare region. The peak X-ray luminosity in 0.3–10 keV band during flare F1 was derived to be $30.4^{+0.5}_{-0.5}\times10^{31}$ erg s^{-1}, which was $\sim$798 times more luminous than the post-flare regions, and $\sim$3378 times more luminous than the quiescent state of CC Eri derived by Pandey & Singh (2008). In order to estimate the amount of soft X-ray luminosity during the time segments when only BAT data were collected, for both the flares, we extrapolated the 14–50 keV luminosity derived from the best-fit APEC model of the BAT data to the 0.3–10 keV luminosity (shown by solid triangle in the top panel of Fig 3).

3.4 XRT+BAT Spectral Analysis

In order to investigate time-evolution in spectral parameters in a 0.3–50 keV range, we performed a time-resolved spectroscopy of flare F1 with a joint spectral fit of XRT and BAT data. We chose seven time-bins (P3–P9) with the same duration used in the spectral fitting of only XRT data described in the previous section (see Fig. 1). In order to derive "effective" coronal parameters for flare emission only we have fitted three temperature APEC model, with a frozen background contribution of first two thermal components. We also added a fourth temperature APEC component in order to explore the possibility of having other temperature plasma, which does not show any further improvements in χ^2. Since galactic HI column density was not found to be variable during only-XRT spectral analysis; therefore, we fixed N_H to its quiescent state value. The global abundances, temperature and corresponding emission measures of the third component were free parameters in spectral fitting. The variations of the spectral parameters are shown in Fig. 3. The peak temperature derived in this spectral fitting is found to

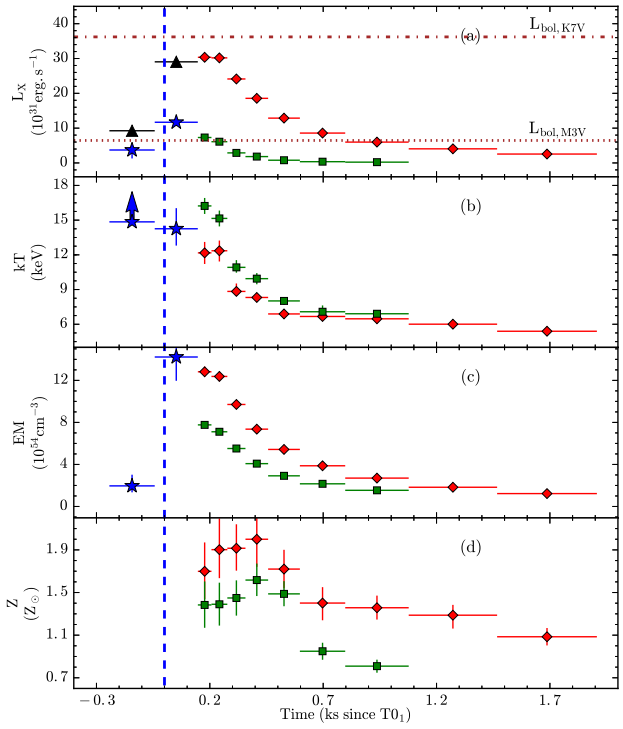

Figure 3: Evolution of spectral parameters of CC Eri during the flare F1. Parameters derived with XRT, BAT, and XRT+BAT spectral fitting in all the panels are represented by solid diamonds, solid stars, and solid squares, respectively. In top panel (a) the X-ray luminosities are derived in 0.3–10 keV (solid diamond), and 14–50 keV (solid star and solid squares) energy band. For first two segments, BAT luminosity derived in 14–50 keV energy band is extrapolated to 0.3–10 keV energy band (solid triangles). The dashed-dotted and dotted horizontal lines correspond to bolometric luminosity of the primary and secondary components of CC Eri, respectively. Panels (b), (c), and (d) display the variations of plasma temperature, emission measure, and abundance, respectively. The dashed vertical line indicates the trigger time of the flare F1. Horizontal bars give time range over which spectra were extracted; vertical bars shows 68% confidence interval.

be $15.8^{+0.7}_{-0.7}$ keV, which is higher than the highest temperature derived from XRT spectral analysis, whereas the peak emission measure and abundance were found to be ∼1.6 and ∼1.2 times lower than to those from XRT data.

3.5 Hydrodynamic modeling of flare decay

The stellar flares, although are not spatially resolved, it is possible to infer the physical size and the structures of the flares by solar analogy using the flare loop models. Using hydrodynamic simulations of semi-circular flaring loops with constant cross-section, and including the effect of the heating in the decay phase of the flare Reale *et al.* (1997) derived an empirical formula of loop-length:

$$L = \frac{\tau_d \sqrt{T_{\max}}}{1.85 \times 10^{-4} F(\zeta)} \qquad F(\zeta) \geq 1 \qquad (1)$$

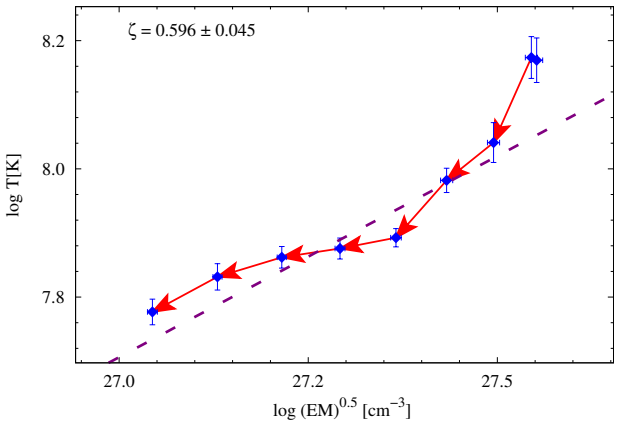

Figure 4: Evolution of flare F1 in log $\sqrt{\mathrm{EM}}$ – log T plane. The dashed line shows the best-fit during the decay phase of the flares with a slope ζ shown in top left corner of each plot.

where L is the loop-length in cm, $T_{\max}$ is the maximum temperature (K) of the loop apex, and $F(\zeta)$ is a non-dimensional factor which provides a quantitative diagnostic of the ratio between the observed decay time (τ_d) and thermodynamic cooling time (τ_{th}). The actual functional form of the parameter $F(\zeta)$ depends on the bandpass and spectral response of the instruments. For *Swift* XRT observations the $F(\zeta)$ was calibrated by Osten *et al.* (2010) as

$$\frac{\tau_{\rm d}}{\tau_{\rm th}} = F(\zeta) = \frac{1.81}{\zeta - 0.1} + 0.67 \qquad (2)$$

which is valid for $0.4 < \zeta \lesssim 1.9$. For stellar observations no density determination is normally available; therefore, we used the quantity $\sqrt{EM}$ as a proxy of the density under the assumption that the geometry of the flaring loop during the decay. Fig. 4 shows the decay-path log $\sqrt{EM}$ versus log T for flares F1. A linear fit to the data provided a slope (ζ) 0.596 ± 0.045, indicating the presence of sustained heating during the decay phase of both flares.

The relationship between the $T_{\max}$ and the observed peak temperature ($T_{\rm obs}$) was also calibrated for *Swift* XRT by Osten *et al.* (2010) as $T_{\max} = 0.0261 \times T_{\rm obs}^{1.244}$, where both temperatures are in K. The $T_{\max}$ was found to be $3.42 \pm 0.55 \times 10^8$ K and the flaring loop-length was derived to be $1.25 \pm 0.13 \times 10^{10}$ cm. Assuming semi-circular geometry, the flaring loop height (L/π) was estimated to be 0.09 and 0.14 times of the stellar radius ($R_\star$) of the primary and secondary of CC Eri. The derived loop lengths were much smaller than the pressure scale height[3] of the flaring plasma of CC Eri; therefore, we can assume that the flaring loop to be not far from a steady state condition. We applied the RTV scaling laws (Rosner *et al.*, 1978) to determine the maximum pressure (p) in the loop at the flare peak and found to be $\sim 12 \times 10^5$ dyne.cm^{-2}. The plasma density (n_e), the flaring volume (V), and the minimum magnetic field (B) to confine the flaring

[3]The pressure scale height is defined as $h_{\rm p} = 2kT_{\max}/(\mu g)$, where μ is the average atomic weight and g is the surface gravity of the star. Considering both the stellar components the derived values of $h_{\rm p}$ are $\geq 9 \times 10^{11}$ cm for flare F1.

plasma were derived as:

$$n_e = \frac{p}{2\,k\,T_{\max}}\ \ \mathrm{cm}^{-3};\quad V = \frac{EM}{n_e^2}\ \ \mathrm{cm}^3;$$
$$B = \sqrt{8\pi\,p}\ \ \mathrm{G} \qquad (3)$$

The estimated values of n_e, V and B during the flare were $12\pm9\times10^{12}$ cm^{-3}, 8.3×10^{28} cm^3, and $\sim$5.4 kG, respectively. Using the scaling laws of Rosner *et al.* (1978), we have also estimated the heating rate per unit volume ($E_H = \frac{dH}{dVdt} \simeq 10^5\,p^{7/6}\,L^{-5/6}$) at the peak of the flare as $\simeq4.8\times10^3$ erg cm^{-3} s^{-1}. The total heating rate ($\frac{dH}{dt} \simeq \frac{dH}{dVdt}\times V$) at the peak of the flare, was derived to be $\sim39.8\times10^{31}$ erg s^{-1}, which is $\sim$1.3 times higher than the flare maximum luminosity. This result is compatible with X-ray radiation being one of the major energy loss terms during the flare. If we assume that the heating rate is constant throughout the decay phase of the flare, the total energy radiated during the flare is given by $E_{\mathrm{X,tot}} > \frac{dH}{dt}\times(\tau_d)$, and derived to be $>2.1\times10^{35}$ erg, which is $\sim$59 s of bolometric energy output of the primary and $\sim$332 s of bolometric energy output of the secondary.

4 Discussions and Conclusion

In this paper, we have presented a superflare observed on an active binary system CC Eri with the *Swift* satellite, which is remarkable in its peak luminosity enhancement in soft and hard X-ray energy bands. A total of eight flares were detected in X-ray bands on CC Eri thus far, out of which the flare discussed in this paper, is the strongest flare in terms of energy released. The soft X-ray luminosity reaches up to $\sim$3378 times more than to that of the quiescent value, which is much larger than any of the previously reported flares on CC Eri observed with *MAXI* GCS ($\sim$5–6 times more than quiescent; Suwa *et al.*, 2011), *Chandra* ($\sim$11 times more than quiescent; Nordon & Behar, 2007), *XMM-Newton* ($\sim$2 times more than quiescent; Pandey & Singh, 2008; Crespo-Chacón *et al.*, 2007), *ROSAT* ($\sim$2 times more than quiescent; Pan & Jordan, 1995) and other flares observed with *EXOSAT* (Pallavicini *et al.*, 1988), *Einstein* IPC (Caillault *et al.*, 1988), and *HEAO1* (Tsikoudi, 1982). However, similar magnitude flares have been reported in the other stars such as DG CVn (Fender *et al.*, 2015), EV Lac (Osten *et al.*, 2010; Favata *et al.*, 2000), II Peg (Osten *et al.*, 2007), UX Ari (Franciosini *et al.*, 2001), AB Dor (Maggio *et al.*, 2000), Algol (Favata & Schmitt, 1999), and EQ1839.6+8002 (Pan *et al.*, 1997). Considering that the flare had happened in the primary (K7.5V), the peak X-ray luminosity of flare F1 was found to be 84% of bolometric luminosity ($\mathrm{L_{bol}}$); if the flare had happened in the secondary (M3.5V) star, the peak X-ray luminosity was 469% of $\mathrm{L_{bol}}$, whereas, the peak luminosity was found to be 71% of combined $\mathrm{L_{bol}}$. During the flare F1, the temperature reached a maximum value of $\sim$342 MK, which is quite high from previously observed maximum flare temperature derived with *Chandra* (Nordon & Behar, 2007) and *XMM-Newton* (Pandey & Singh, 2008; Crespo-Chacón *et al.*, 2007), but this value is of the similar order to those of the other superflares detected on EV Lac ($\approx$150 MK and $\approx$142 MK; Favata *et al.*, 2000; Osten *et al.*, 2010), II Peg ($\approx$300 MK; Osten *et al.*, 2007), and AB Dor ($\approx$114 MK; Maggio *et al.*, 2000). The peak abundances are found to enhance $\sim$11 times more than that of the quiescent value. During other superflares, abundances were found to increase between 2–3 times more than that of the quiescent level (Favata *et al.*, 2000; Favata & Schmitt, 1999; Maggio *et al.*, 2000). But the superflare observed with *Swift* in EV Lac, the abundances were found to remain constant throughout the flare. With hydrodynamic modeling, we derived the loop length of both flares to be $\sim1.3\times10^{10}$ cm, which is $\sim$2.2 times larger than two previously observed flares by *XMM-Newton* satellite (Crespo-Chacón *et al.*, 2007) on CC Eri. The loop lengths are also in between the loop lengths derived for other G–K dwarfs, dMe stars and RS CVn type binaries (e.g. Favata & Micela, 2003; Pandey & Singh, 2008, 2012). The heating rate during the flare F1 is also found to be $\sim$93% of the bolometric luminosity of the CC Eri system. Under the assumptions that the energy release is indeed of magnetic origin, the total non-potential magnetic field B_0 involved in a flare energy release within an active region of the star can be obtained from the relation:

$$E_{\mathrm{X,tot}} = \frac{(B_0^2 - B^2)}{8\pi}\times V \qquad (4)$$

Assuming that the loop geometry does not change during the flare, B_0 is estimated to be $>$9.7 kG. Although we have used the loop volume in the derivation of B_0, this is not to imply that the field fills up the whole volume. Rather, our estimates can be interpreted as the flare energy stored in a magnetic field configuration (e.g. a large group of spots) with a field strength of several kG, covering a volume comparable to the one of the flaring loop. Bopp & Evans (1973) has estimated a magnetic field of 7 kG on CC Eri at photospheric level. Most dynamo theories suggest (Durney *et al.*, 1993) that less magnetic flux should be generated by a turbulent dynamo as compared to the case of the solar-type "shell" dynamo, because there is no stable overshoot layer where the fields can be stored and amplified. This suggests that the flares might happen most likely on the corona of the primary K7.5-type, rather than the secondary M3.5-type. However, M-type star EV Lac (Favata *et al.*, 2000) and few other M-dwarfs (Shulyak *et al.*, 2014) shows very high surface magnetic fields, which can not be explained with an hypothesis of the M-type stars are fully convective. In this scenario, it is very difficult to identify the component of the binaries on which the flares have happened.

Thus with *Swift* BAT and XRT instrument we have analysed a superflare on CC Eri, which is the first superflare ever identified on this object, and gives a useful information about the upper extreme of magnetic activities. We also have detected Fe Kα line emission during different time-segments of the flare. Details study of the superflare will be published elsewhere (Karmakar et al. 2016).

Acknowledgments

This work made use of data supplied by the UK Swift Science Data Centre at the University of Leicester. This research has made use of the XRT Data Analysis Software (XRTDAS) developed under the responsibility of the ASI Science Data Center (ASDC), Italy.

Facilities: Swift (BAT), *Swift* (XRT).

References

Amado, P. J., Doyle, J. G., Byrne, P. B., Cutispoto, G., Kilkenny, D., *et al.* 2000, A&A, 359, 159.

Anders, E. & Grevesse, N. 1989, Geochimica Cosmochimica Acta, 53, 197.
Arnaud, K. A. 1996, In *Astronomical Data Analysis Software and Systems V*, edited by G. H. Jacoby & J. Barnes, *Astronomical Society of the Pacific Conference Series*, vol. 101, p. 17.
Barthelmy, S. D., Barbier, L. M., Cummings, J. R., Fenimore, E. E., Gehrels, N., *et al.* 2005, SSRv, 120, 143.
Barthelmy, S. D., Baumgartner, W. H., Chester, M. M., Gehrels, N., Holland, S. T., *et al.* 2012, GRB Coordinates Network, 12985.
Bopp, B. W. & Evans, D. S. 1973, MNRAS, 164, 343.
Burrows, D. N., Hill, J. E., Nousek, J. A., Kennea, J. A., Wells, A., *et al.* 2005, SSRv, 120, 165.
Busko, I. C., Quast, G. R., & Torres, C. A. O. 1977, A&A, 60, L27.
Caillault, J.-P., Drake, S., & Florkowski, D. 1988, AJ, 95, 887.
Crespo-Chacón, I., Micela, G., Reale, F., Caramazza, M., López-Santiago, J., *et al.* 2007, A&A, 471, 929.
Demircan, O., Eker, Z., Karataş, Y., & Bilir, S. 2006, MNRAS, 366, 1511.
Dickey, J. M. & Lockman, F. J. 1990, ARA&A, 28, 215.
Durney, B. R., De Young, D. S., & Roxburgh, I. W. 1993, SoPh, 145, 207.
Emslie, A. G., Kucharek, H., Dennis, B. R., Gopalswamy, N., Holman, G. D., *et al.* 2004, Journal of Geophysical Research (Space Physics), 109, A10104.
Evans, D. S. 1959, MNRAS, 119, 526.
Evans, P. A., Page, K. L., Beardmore, A. P., Osborne, J. P., Godet, O., *et al.* 2008, The Astronomer's Telegram, 1787.
Favata, F. & Micela, G. 2003, SSRv, 108, 577.
Favata, F., Reale, F., Micela, G., Sciortino, S., Maggio, A., *et al.* 2000, A&A, 353, 987.
Favata, F. & Schmitt, J. H. M. M. 1999, A&A, 350, 900.
Fender, R. P., Anderson, G. E., Osten, R., Staley, T., Rumsey, C., *et al.* 2015, MNRAS, 446, L66.
Franciosini, E., Pallavicini, R., & Tagliaferri, G. 2001, A&A, 375, 196.
Godet, O., Beardmore, A. P., Abbey, A. F., Osborne, J. P., Cusumano, G., *et al.* 2009, A&A, 494, 775.
Maggio, A., Pallavicini, R., Reale, F., & Tagliaferri, G. 2000, A&A, 356, 627.
Moretti, A., Campana, S., Mineo, T., Romano, P., Abbey, A. F., *et al.* 2005, In *UV, X-Ray, and Gamma-Ray Space Instrumentation for Astronomy XIV*, edited by O. H. W. Siegmund, *Society of Photo-Optical Instrumentation Engineers (SPIE) Conference Series*, vol. 5898, pp. 360–368.
Morrison, R. & McCammon, D. 1983, ApJ, 270, 119.
Nordon, R. & Behar, E. 2007, A&A, 464, 309.
Osten, R. A., Drake, S., Tueller, J., Cummings, J., Perri, M., *et al.* 2007, ApJ, 654, 1052.
Osten, R. A., Godet, O., Drake, S., Tueller, J., Cummings, J., *et al.* 2010, ApJ, 721, 785.
Pallavicini, R., Monsignori-Fossi, B. C., Landini, M., & Schmitt, J. H. M. M. 1988, A&A, 191, 109.
Pan, H. C. & Jordan, C. 1995, MNRAS, 272, 11.
Pan, H. C., Jordan, C., Makishima, K., Stern, R. A., Hayashida, K., *et al.* 1997, MNRAS, 285, 735.
Pandey, J. C. & Singh, K. P. 2008, MNRAS, 387, 1627.
Pandey, J. C. & Singh, K. P. 2012, MNRAS, 419, 1219.
Reale, F., Betta, R., Peres, G., Serio, S., & McTiernan, J. 1997, A&A, 325, 782.
Rosner, R., Tucker, W. H., & Vaiana, G. S. 1978, ApJ, 220, 643.
Schaefer, B. E., King, J. R., & Deliyannis, C. P. 2000, ApJ, 529, 1026.
Shibata, K. & Yokoyama, T. 2002, ApJ, 577, 422.
Shibayama, T., Maehara, H., Notsu, S., Notsu, Y., Nagao, T., *et al.* 2013, ApJS, 209, 5.
Shulyak, D., Reiners, A., Seemann, U., Kochukhov, O., & Piskunov, N. 2014, A&A, 563, A35.
Smith, R. K., Brickhouse, N. S., Liedahl, D. A., & Raymond, J. C. 2001, ApJL, 556, L91.
Suwa, F., Asada, M., Sugizaki, M., Negoro, H., Mihara, T., *et al.* 2011, The Astronomer's Telegram, 3837.
Tsikoudi, V. 1982, ApJ, 262, 263.